Insulin Receptor Loss Impairs Mammary Tumorigenesis in Mice

Lauren Podmore[1,‡], Yekaterina Poloz[2,3,‡], Samar Mouaaz[2], Marguerite Ennis[4], Petr Smirnov[1], Sonya Lam[2], Ryan Dowling[2,3], Vuk Stambolic[1,2,*]

Abstract

Breast cancer (BC) prognosis and outcome are adversely affected by increased body weight, obesity and the obesity-associated type 2 diabetes. Hyperinsulinemia, which is commonly seen as part of metabolic reprograming in the obese state, has been associated with higher risk of death and recurrence in BC. Up to 80% of breast cancers overexpress the insulin receptor (INSR) *de novo*, which correlates with worse prognosis. To directly probe the role of insulin signaling in mammary tumorigenesis in the mouse, we generated the MMTV-driven polyoma middle T (PyMT) and ErbB2/Her2 BC models, respectively, with coordinate mammary epithelium-restricted deletion of the INSR. In both models, deletion of either one or both copies of the INSR in the mammary gland led to a marked delay in tumor onset and burden, including in mice fed to mimic conditions of human obesity. Longitudinal monitoring of generated mouse models revealed that tumor initiation, rather than progression and metastasis, were impacted by INSR deletion. The similarity of phenotypes elicited by the deletion of one or both copies of INSR raises the possibility that there is a dose-dependent threshold for the contribution of INSR to mammary tumorigenesis.

Affiliations:

1: Department of Medical Biophysics, University of Toronto, Princess Margaret Cancer Research Tower, Toronto, Ontario, Canada M5G 1L7.

2: Princess Margaret Cancer Centre, University Health Network, Princess Margaret Cancer Research Tower, Toronto, Ontario, Canada M5G 1L7.

3: Current address: F. Hoffmann-La Roche Ltd, Mississauga, Ontario, Canada L5N 5M8.

4: Applied Statistician, Markham, Ontario, Canada, L3R 6H9.

‡These authors contributed equally to this work

*Corresponding Author:

Vuk Stambolic

Princess Margaret Cancer Centre, University Health Network, Princess Margaret Cancer Research Tower, Room 13-313, 101 College Street, Toronto, Ontario, Canada M5G 1L7.

E-mail: vuks@uhnresearch.ca

Running Title: Investigating the function of INSR in mammary tumourigenesis

Key words: insulin receptor, BC, mammary tumourigenesis, genetically engineered mouse model

Introduction

Obesity is a global epidemic, with over 650 million obese and further 1.3 billion overweight individuals worldwide[1]. 5% and 10% of all US cancer cases in men and women, respectively, can be attributed to excess body weight[2]. Estimates from almost two decades ago attribute obesity to approximately 14% of the deaths from cancer in men and 20% of the deaths from cancer in women[3]. In breast cancer (BC), for each 5 kg/m^2 increase in body mass index (BMI), risk of BC–specific mortality increased by 17-29%[4]. Importantly, sustained weight loss is associated with lower BC risk in women 50 or older, indicating that the effects of excess body weight on BC are reversible[5].

Elevated levels of circulating insulin, or hyperinsulinemia, a condition that parallels obesity[6], has an adverse effect on a patient's prognosis and risk in operable BC[7–10]. Further, there is a positive association between cancer incidence and insulin dose in persons with type 2 diabetes treated by both human insulin and synthetic insulin analogues[11]. Adverse effects of insulin and benefits of insulin deprivation in a rat model of mammary tumorigenesis have been shown half a century ago[12,13]. More recently, excess insulin was found to accelerate mammary tumorigenesis in mouse models, whereas insulin reducing agents counter it[14,15]. Importantly, in a pancreatic cancer mouse model, hyperinsulinemia accelerated tumorigenesis, whereas genetically-mediated insulin reduction decelerated tumorigenesis, separating the impact of elevated insulin on tumor growth from the accompanying hyperglycemia seen in metabolic disease[16].

Immunohistochemical analyses have revealed that more than 80% of breast tumours overexpress the insulin receptor (INSR)[17,18], a heterotetrameric receptor

tyrosine kinase typically found in muscle, fat and liver cells, where it propagates metabolic signalling[19]. While metabolic tissues express the INSR-B isoform, cancers predominantly express INSR-A, the foetal INSR isoform capable of mediating mitogenic signaling[20]. Engagement of insulin with INSR results in activation of the PI3K signaling pathway, an anabolic cascade central to the control of glucose transport across cell membranes, glycolysis, lipolysis, mRNA translation and cell growth, survival and migration[21]. Hyperactivation of PI3K signaling is found in many human tumours, largely owing to the activating mutations in PIK3CA, the catalytic subunit of PI3K, and loss of function of the tumor suppressor PTEN, which counters PI3K signaling via its lipid phosphatase activity against phosphatidylinositol second messengers produced by PI3K[22]. Moreover, insulin stimulation of INSR-A also activates the pro-mitogenic Ras/Erk signaling cascade[23].

To understand the function of insulin signaling in mammary tumorigenesis, we genetically disrupted the INSR gene in mammary tissues of two mouse models of BC, driven by the polyoma middle T (PyMT) and ErbB2/Her2 oncogenes, respectively. Our data demonstrate that INSR loss impairs mammary tumor initiation, but not progression or metastasis, and suggest the existence of a dose-dependent threshold for the contribution of INSR to mammary tumorigenesis.

Materials and Methods

Dataset for Human Samples and Cell Lines

RNASeq gene expression data from both TCGA (The Cancer Genome Atlas)[24,25] and CCLE (Cancer Cell Line Encyclopedia)[26] were obtained from the web-based program UCSC Xena[27]. Box-plots, Kaplan-Meier survival plots, scatter-plots and p-values of these data were visualized and calculated using Graphpad Prism 7.

Cell culture

MCF-10A cells were cultured in DMEM/F12 (Invitrogen #11330-032) supplemented with 5% fetal bovine serum (FBS), 20 ng/mL epidermal growth factor, 0.5 mg/mL hydrocortisone, 100 ng/mL cholera toxin, 10 µg/mL insulin and 1% penicillin/streptomycin[28]. HEK-293T, MCF-7 and MDA-MB-231 cells were cultured in DMEM (Invitrogen #D5796-500ML) supplemented with 10% FBS and 1% penicillin/streptomycin. For immunoblot signalling analyses, MCF-10A cells were seeded in above culture medium (Basal), followed by either basal medium replenishment or overnight starvation with DMEM/F12 supplemented with only 0.5 mg/mL hydrocortisone, 100 ng/mL cholera toxin and 1% penicillin/streptomycin (Starved). These cells were then stimulated with 10 µg/mL insulin in either the absence (Starved + Ins) or presence (Starved + OSI + Ins) of pre-treatment with 1 µM linsitinib (OSI-906) for 2 hours. For shRNA analyses, MCF10A cells were transduced with lentiviral pLKO.1 puromycin shRNA vectors (RNAi Consortium, Broad Institute) to target expression of INSR (shRNA1 = 5’-GTG-CTG-TAT-GAA-GTG-AGT-TAT-3’, shRNA2 =

5’-CTC-GTT-TGG-TTA-CCA-ATT-TAA-3’), PIK3R1 (shRNA1 = 5’-ACA-TCG-CAC-TGT-GGA-TTA-TTT-3’, shRNA2 = 5’-TTC-ATC-GAG-ATG-GGA-AAT-ATG-3’) and SHC1 (shRNA1 = 5’-CCA-CGG-GAG-CTT-TGT-CAA-TAA-3’, shRNA2 = 5’-TGA-CCA-TCT-CTT-AGG-TCT-AAT-3’), or a non-targeting control (shGFP, 5'-GCA-AGC-TGA-CCC-TGA-AGT-TCA-T-3'), followed by growth in either Basal, Starved or Starved + Ins conditions outlined above.

PCR

Cells were grown under normal culture conditions followed by lysis with TRIzol Reagent (Invitrogen # 15596026), phase separation with chloroform, and RNA precipitation with isopropanol. RNA was then washed with 70% ethanol and re-dissolved with DEPC-treated water. First-strand cDNA synthesis from isolated mRNA was performed as outlined in the protocol for Superscript III Reverse Transcriptase (Invitrogen #18080051). For cDNA isolated from HEK-293T, MCF-10A, MCF-7 and MDA-MB-231 cells, polymerase chain reaction (PCR) was performed using primers spanning INSR exon 11 (Fwd: 5’-AAC-CAG-AGT-GAG-TAT-GAG-GAT-3’; Rev: 5’-CCG-TTC-CAG-AGC-GAA-GTG-CTT-3’) to specifically detect INSR isoforms as previously described[29]. PCR products were separated by gel electrophoresis and densitometry analysis of bands representing INSR-A (exon 11-, 600 bp) and INSR-B (exon 11+, 636 bp) allowing for relative INSR isoform expression levels to be calculated using Graphpad Prism 7. For shRNA knockdown experiments in MCF-10A cells, real-time PCR (RT-PCR) was performed using primers targeting INSR (Fwd: 5’-AAC-CAG-AGT-GAG-TAT-GAG-GAT-3’; Rev: 5’-CGT-TCC-AGA-GCG-AAG-TGC-TT-3’), PIK3R1

(Fwd: 5’-CGC-CTC-TTC-TTA-TCA-AGC-TCG-TG-3’, Rev: 5’- GAA-GCT-GTC-GTA-ATT-CTG-CCA-GG-3’) and SHC1 (Fwd: 5’- ACA-GCC-GAG-TAT-GTC-GCC-TAT-G-3’, Rev: 5’-CAA-TGG-TGC-TGA-TGA-CAT-CCT-GG-3’), with expression levels of RPLPO (Fwd: 5'- CAA-CCC-TGA-AGT-GCT-TGA-CAT-3', Rev: 5'-AGG-CAG-ATG-GAT-CAG-CCA-3') used as a loading control. Fold change in mRNA expression between shRNA-treated and untreated cells was calculated and visualized in Graphpad Prism 7.

Immunoblotting

To prepare total protein lysates, cells were homogenized in CHAPS lysis buffer (0.3% CHAPS, 120 mM NaCl, 1x protease inhibitor cocktail in 1.5 mM HEPES buffer pH 7.5). To detect relative protein and phosphorylated protein levels, immunoblots were probed with antibodies against INSR (Millipore Sigma #07-724), phospho-INSR/IGF1R (Y1135/1136, Cell Signaling #3024), Akt (Cell Signaling #4691), phospho-AKT (S^{473}) (Cell Signaling #4058), ERK (Cell Signaling #9102), phospho-p44/42 MAPK (Erk1/2) (T^{202}/Y^{204}) (Cell Signaling #9101), S6 (Cell Signaling #2217), phospho-S6 (S235/S236, Cell Signaling #), and p85α (Cell Signaling #4292). GAPDH (Santa Cruz #sc-25778) was probed for as a loading control.

Conditional INSR deletion in *MTB:MIC* or *NIC* BC mouse models

The animals used in these experiments were housed in the UHN animal facilities accredited by the Canadian Council on Animal Care and treated in accordance with the institutional guidelines and the UHN Animal Care Committee-approved protocols. *MMTV-rtTA* mice were a generous gift of Dr. Lewis A. Chodosh from the University of

Pennsylvania School of Medicine[30]. *PyMT-IRES-Cre* mice were a generous gift of Dr. William Muller from the Rosalind and Morris Goodman Cancer Research Centre at McGill University[31]. *MMTV-NIC* (*NIC*) mice were a generous gift of Dr. Giuseppina Ursini-Siegel from the Lady Davis Institute for Medical Research at McGill University[32]. *INSR*$^{F/F}$ (B6.129S4(FVB)-*Insr*^{tm1Khn}/J; stock #006955) and *FVB/NJ* mice (stock #001800) were purchased from the Jackson Laboratory. *INSR*$^{F/F}$ were backcrossed onto the *FVB/NJ* background for 6 generations. Mice were genotyped using the following primers: MMTV-rtTA (Fwd: 5' ACC GTA CTC GTC AAT TCC AAG GG 3', Rev: 5' CGC CAT TAT TAC GAC AAG 3'), PyMT-IRES-Cre (Fwd: 5' GGA AGC AAG TAC TTC ACA AGG G 3', Rev: 5' GGA AAG TCA CTA GGA GCA GGG 3'), neu (Fwd: 5′-CCT CTG ACG TCC ATC GTC TC-3′, Rev: 5′-CGG ATC TTC TGC TGC CGT CG-3′), and the conditional INSR allele (Fwd: 5' GAT GTG CAC CCC ATG TCT G 3', Rev: 5' CTG AAT AGC TGA GAC CAC AG 3'). Regular chow-fed *MMTV-rtTA/PyMT-IRES-Cre/INSR*$^{+/+,\ F/+\ or\ F/F}$ (*MTB:MIC INSR* (+/+), (F/+) or (F/F)) mice were administered 2 mg/mL doxycycline (Sigma-Aldrich) in their drinking water at 10-12 weeks of age. Alternatively, *MTB:MIC:INSR*$^{+/+,\ F/+\ or\ F/F}$ mice were fed a high-fat diet (#7012, Teklad Diets) for 10 weeks before the doxycycline administration. *MTB:MIC INSR* (+/+), (F/+) or (F/F) mice were sacrificed at a fixed end-point of 8 weeks or 10 weeks post doxycycline administration. *NIC INSR* (+/+), (F/+) or (F/F) mice were fed regular chow and monitored weekly for palpable tumours; upon detection, weekly caliper measurements were performed until a humane endpoint was reached (total tumour volume ≥ 1000 mm^3), followed immediately by sacrifice. For both mouse models, mammary tumours, lungs and other tissues were excised, weighed (tumours only), counted (tumours only)

and fixed in 5% formalin for 48 hr at 4º C. Post-fixation, tumours and tissues were rinsed with PBS and stored in 70% ethanol at 4º C. Visualization and statistical analysis of all measurements were performed in GraphPad Prism 9.

Statistical modeling and analysis of tumour growth data

Tumour growth data from *NIC:INSR* mice was filtered to ensure that all tumours considered had at least two measurements before the mouse was sacrificed. Visual examination of the data suggested an exponential growth pattern for the tumours. To directly test for this, both linear and log-linear mixed models were fit to the measured tumour volume data over time to estimate the average tumour growth rate for each mouse. The measured volume of each tumour was modelled as a function of the tumour age, including fixed effect terms for the interaction between the genotype and the age of the tumour, as well as a fixed effect intercept for each genotype. Random effects were included for the mouse to mouse variation in the slope of the model, and for the tumour to tumour variation in the intercept. The model estimated an average tumour growth rate (linear or exponential) for each genotype, allowing for random variation in the growth rates between mice. The relationships between the residual and fitted values for the linear and log-linear models were visually examined, with the linear model displaying a pronounced dependency between the residuals and the fitted volume, suggesting a biased fit to the observed data, validating the use of the log-linear model. Estimated percent growth per day values were calculated from the coefficients estimated by the model for each mouse, adding together the average genotype growth rate and the random mouse-specific deviation from the average.

The significance of differences between groups was assessed using a nested-model ANOVA, comparing the full model described to a restricted model which excludes the fixed and random effects of genotype on growth rate (but retains the effect of genotype on the intercept). The tested null hypothesis was that a single average growth rate explains the observed data, as well as an average growth rate fit to each genotype separately. Two group comparisons were done by first refitting both models to the subset of the data belonging to the two compared groups.

The same data were also analysed after summing the tumour volumes for each mouse, calculating total tumour volume per mouse. Note that the previous analysis estimated an intercept term for each tumour, meaning the slopes were fit after adjusting for the different time of tumour onset. In per mouse analysis, the volume of tumours arising from the same mouse is added to the mouse total as they arise. For modelling these data, the models described above were modified to fit one random intercept per mouse. The same approach was taken for this analysis: after visual examination, linear and log-linear mixed models were fit to the data and compared based on a bias of residuals based on fitted total tumour volumes. As in per tumour analysis, the log-linear model was found to be a better fit than the linear model. Significance testing was done as above, comparing the explanatory power of models fit using the genotype information to those fitting a single slope for mice from all genotypes.

All models were estimated using the `afex` (1.0-1) (CRAN.R-project.org/package=afex) and `lme4` (1.1-27.1)[33] packages, as implemented in the R Statistical Computing Environment (4.1.2) (R-project.org/). Plots were generated using

the `ggprism` (1.0.3) (CRAN.R-project.org/package=ggprism) and `ggplot2` (3.3.5) (ggplot2.tidyverse.org) packages.

Immunohistochemistry and semi-automated digital image analysis

For histopathological and signaling analyses, FFPE tumours of *MTB:MIC* and *NIC INSR* mice collected at endpoint were sectioned and stained with hematoxylin and eosin (H&E), or probed with antibodies against INSR (Upstate #05-1104), IGF1R (Cell Signalling #3027), HER2 (Santa Cruz #284), phospho-AKT (S^{473}) (p-AKT; Cell Signaling #4058), phospho-p44/42 MAPK (Erk1/2) (T^{202}/Y^{204}) (p-ERK; Cell Signaling #9101), and Ki67 (Lab Vision #RM-9106-S1, clone SP6) by the Applied Molecular Profiling Laboratory and the Pathology Research Program at UHN. All slides were digitized for subsequent quantification by image analysis.

INSR, IGF1R, p-AKT, p-ERK and Ki67 stains were quantified using QuPath bioimage analysis software (Bankhead et al., 2017). Briefly, images of all slides of a given stain were loaded into a single project file where stain vector and background estimates for each antibody were used to improve stain separation using colour deconvolution. *Simple Tissue Detection* command was used to batch process the selection of tissue from tumour sections and exclusion of white space on all project slide images, followed by manual annotation of each tissue sample and exclusion of any stain artifact. The *Positive Cell Detection* command, which detects paired nuclei and cell boundaries within an annotation and scores each cell for staining intensity, was run with its parameters manually set and intensity thresholds optimized for each stain based upon mean nuclear (Ki67), cytoplasm (INSR, IGF1R, p-AKT) and cell (p-ERK) DAB

optical densities of positive and negative control annotations. All project annotations were then batch processed with the optimized *Positive Cell Detection* parameters, followed by tissue classification using a Random Forest Classifier trained on manual annotations of tumour or stomal cells which finally enumerated tumour tissue-specific cells that were either negative (0 < lowest intensity threshold parameter) or positive (weak (1+) ≥ lowest intensity threshold parameter; moderate (2+) ≥ 2-fold 1+; strong (3+) ≥ 3-fold 1+) for a stain. Tumour % Positivity and Tumour H-scores for each annotation were quantified by QuPath, with subsequent visualization and statistical analysis performed in GraphPad Prism 9. Representative images of stained sections were visualized in QuPath at 20X magnification.

To validate tissue-specificity of the INSR knockout, FFPE liver, muscle and adipose (fat) tissues in *MTB:MIC* INSR (+/+) and (F/F) mice were sectioned, stained with anti-INSR and digitized for image visualization. To count metastases for both *MTB:MIC* and *NIC* mice, FFPE lungs collected at endpoint were serially sectioned (5 µm sections, 100 µm apart) and stained with H&E, followed by digitization and analysis using Aperio ImageScope (Leica Biosystems). The number of metastases were averaged across 5 sections, with subsequent visualization and statistical analysis performed in GraphPad Prism 9.

Blood glucose and insulin concentrations in INSR knockout mice

To ensure that INSR signaling was intact in the metabolic tissues of INSR knockout mice, their blood glucose and plasma insulin concentrations were measured. Mice were deprived of food for 6 hours, at which time blood glucose concentrations

were measured using Accu-Chek Performa test strips and meter (Roche, Indianapolis, IN, USA). The mice were then bled and euthanized according to ethics guidelines of UHN, plasma insulin concentrations were determined by rodent-specific insulin ELISA kit (Millipore #EZRMI-13K). For the glucose tolerance test, mice were deprived of food for 6 hours, then injected with 2 g/Kg glucose into the intraperitoneal cavity. Blood glucose concentrations were measured as described previously at 0, 15, 30, 60 and 120 minutes post-injection[34]. Visualization and statistical analysis of all measurements were performed in GraphPad Prism 9.

Results

INSR is broadly expressed in human cancer and regulates PI3K/Akt and Ras/ERK signaling pathways in mammary epithelial cells.

To expand on the previous immunohistochemical analyses of INSR expression in BC, we analyzed gene expression of INSR (by RNASeq) from The Cancer Genome Pan-Cancer Atlas (TCGA PANCAN) dataset[24,25]. Levels of INSR mRNA expression in BC were increased relative to more than half of other obesity-linked cancers (**Figure 1A**), and to three-quarters of all cancer types (**Supplementary Figure 1A**). INSR mRNA expression varied amongst both histological (**Figure 1B**) and molecular (**Figure 1C**) BC subtypes, but not TMN stage (**Supplementary Figures 2F-I**) and was highest in invasive lobular carcinomas and the luminal A molecular subtype, corroborated by the observation of higher INSR expression in tumours positive for either estrogen receptor (ER; **Supplementary Figure 2C**) or progesterone receptor (PR; **Supplementary Figure 2D**). Interestingly, while there was no difference in INSR expression in normal breast tissues relative to primary tumours of any histological subtype (**Supplementary Figure 2A**), tumours positive for HER2 saw lower overall INSR expression relative to both normal breast tissue and to HER2 negative tumours (**Supplementary Figures 2B, E**). Of note, although relative INSR expression levels did not impact overall survival in all BC patients (**Supplementary Figure 2J**), higher INSR expression was correlated with poorer survival outcomes in patients with basal BCs (**Figure 1D**).

INSR mRNA expression was also analyzed in BC cell lines from the Cancer Cell Line Encyclopedia dataset[26]. Relative to all cancer lines independent of the primary site, BC-derived cell lines rank within the top third by INSR expression (**Supplementary**

Figure 1B-**C**). INSR isoform mRNA expression within a select group of cell lines was analyzed by qRT-PCR (**Figure 1E**). All cell lines expressed both INSR isoforms, but at differing ratios, INSR-A:INSR-B, respectively, 40:60 in MCF-10A, 80:20 in MCF-7 and MDA-MB-231). On the protein level, INSR abundance in MCF-7 and MDA-MB-231 was comparable to that of kidney cancer-derived HEK-293T cells, whereas MCF-10A cells displayed relatively lower expression (**Figure 1F**).

To probe whether the expressed INSR is functional, MCF10A cells were starved of serum and growth factors and short-term stimulated with insulin. Judging by stimulation-dependent increase in phosphorylation of INSR, AKT, S6 and ERK, insulin led to activation of both the metabolic and mitogenic arms of INSR signaling, reflective of their INSR-A expression. (**Figure 1G**). The effect was INSR-dependent, as S6 and ERK phosphorylation in response to insulin stimulation were attenuated by INSR knockdown, as well as by pre-treatment with an INSR/IGF1R-selective inhibitor OSI-906. (**Supplementary Figure 3A-B**).

INSR contributes to mammary tumourigenesis in BC model mice

To directly investigate the role of INSR in mammary tumorigenesis in mice *in vivo*, we generated two genetically engineered mouse models with conditional mammary tissue-specific deletion of *INSR,* concomitant with expression of either the polyoma middle-T antigen (*MMTV-rtTA;TetO-PyMT-IRES-Cre*, or *MTB:MIC*) or oncogenic HER2 (*MMTV-neu-IRES-Cre*, or *NIC*), respectively (**Figure 2A-B**)[30–32]. In the *MTB:MIC INSR* model, MMTV promoter-dependent PyMT expression/INSR deletion are induced through treatment with doxycycline in the drinking water**,** whereas in *NIC*

animals, Her2 expression and *INSR* deletion are coordinated by the activity of the MMTV promoter. Predicted allele and oncogene representation was monitored by genomic PCR (**Figures 2C-E**). Mammary tumours that developed in both models expressed INSR protein (**Figures 2F-G**), while, consistent with their genotype, INSR was undetectable in mammary tumours of 10-week old *MTB:MIC INSR* and *NIC INSR* mice homozygous for the conditional *INSR* allele (F/F) compared to those wild-type for *INSR* (+/+). Metabolic INSR expressing tissues, such as liver, muscle and fat, displayed unchanged INSR levels, and maintained normal glucose homeostasis (**Figure 2H**) validating specificity of the mammary tissue INSR deficiency.

Cohorts of female mice carrying the respective oncogenes and *INSR* wild-type (+/+), *INSR* heterozygous-null (F/+) and *INSR* null (F/F) were established. At 10-12 weeks of age, PyMT-Cre expression was induced in all *MTB:MIC INSR* mice through doxycycline in the drinking water, and mice in both groups were monitored weekly for presence of tumours by palpation. PyMT induction rapidly led to appearance of tumours (~8 days post induction) in all three *INSR* genotypes. While all *MTB:MIC INSR* (+/+) mice presented with tumours within 30 days post induction, at the 8-week monitoring endpoint, set due to the severity of the tumour phenotypes found in *MTB:MIC INSR* (+/+), a considerable proportion of *MTB:MIC* PyMT *INSR* (F/F) and *MTB:MIC INSR* (F/+) did not show signs of disease or had fewer tumours (**Figure 3A**). Reduction in tumours followed the number of deleted *INSR* copies, with >20% of *MTB:MIC INSR* (F/+) and >40% of *MTB:MIC INSR* (F/F) remaining tumour-free at endpoint.

In *NIC* mice, where cancers take longer to develop, loss of *INSR* delayed tumour appearance in a deleted *INSR* allele-dependent manner, with *NIC INSR* (+/+) tumours

emerging at 133 days, *NIC INSR* (F/+) at 158 days and *NIC INSR* (F/F) at 172 days (**Figure 3B**). Consistently, all *NIC INSR* (+/+) animals developed tumours within 172 days, while it took 294 days for all *NIC INSR* (F/F) mice to show signs of disease. Delayed tumour onset due to INSR deletion was also reflected in the time it took mice to reach the humane endpoint, with *NIC INSR* (F/+) and *NIC INSR* (F/F) displaying substantial survival benefit compared to their *NIC INSR* (+/+) counterparts (**Figure 3C**).

Deletion of a single or both copies of *INSR* also led to remarkably lowered tumour burden in both models, reflected in the number and total weight of mammary tumours at endpoint (**Figures3D-F)**. While *MTB:MIC INSR* (+/+) mice had >20 tumours per mouse on average, both *MTB:MIC INSR* (F/+) and *MTB:MIC INSR (F/F)* featured ~5 tumors per mouse at endpoint (**Figure 3D**). Reduced tumour count paralleled lower total tumour weights in *INSR*-deficient *MTB:MIC* mice at endpoint (**Figure 3E**). Similarly, *NIC INSR* (+/+) mice developed up to 15 tumours per mouse, whereas *NIC INSR* (F/+) and *NIC INSR* (F/F) mice averaged around 5 lesions per mouse (**Figure 3F**).

***INSR* deletion impacts tumor initiation, but not progression and metastasis**

While *MTB:MIC INSR* tumours that escaped the impact of *INSR* loss on initiation appeared to, on average, weigh less at endpoint (**Figure 4A**), this reduction was not statistically significant and the extent of disease in this model precluded further comparisons of the impact on tumour progression. Nevertheless, slower tumour development in *NIC INSR* mice afforded a more detailed assessment of the impact of INSR on tumour progression. Diameters/volumes of individual tumors and total tumors per mouse in the three *NIC INSR* genotypes were recorded weekly by caliper

measurements. Plotting of the growth of individual tumours and cumulative tumour volume per mouse over time suggested non-linear, exponential growth (**Figure 4B, E**). Data were log10 transformed (**Figures 4C, F**) and fit of the linear mixed models to both the original and log-transformed data were compared (see Methods). Fitting to the data on a natural scale showed pronounced dependency between the residuals and the fitted volume, with the model consistently under-estimating the observed data for the smallest and largest volumes, and over-estimating for values in the centre of the range. This was indicative of bias, favoring the use of the log-linear model consistent with exponential tumour growth. Comparison of percent growth per day values for each tumour calculated from the models (>10 per genotype) showed that there was no difference in progression of individual tumors between the genotypes (**Figure 4D**).

To estimate the impact of *INSR* deletion on metastatic spread, number of lung metastases in both models were compared. In both the highly metastatic *MIC:MTB INSR* and more moderate *NIC INSR* models, deletion of either single or both copies of *INSR* had no effect on metastatic dissemination (**Figures 4G-H**). Taken together, these results demonstrate that INSR functionally contributes to mammary tumour initiation, but not progression and metastases in the tested models of BC.

Loss of INSR reduces mammary tumourigenesis in the obese state

Considering that INSR contribution to BC might be of particular significance in the obese and/or hyperinsulinemic patients, the impact of *INSR* deletion on mammary tumourigenesis was also explored in models mimicking these conditions. Consumption of a high fat content diet in several mouse strains, including FVB, is known to cause

metabolic disease[35]. In our lab, compared to those fed a regular fat diet (RFD), FVB/NJ mice fed a diet with high fat content (45% caloric intake from fat) (HFD) for 10 weeks increased their body weight and fared poorer in a glucose tolerance test (**Figure 5A-B**). To use this strategy to induce metabolic disease before tumour initiation, a cohort of *MTB:MIC INSR* mice aged 10 weeks either RFD or HFD for additional 10 weeks, prior to induction of PyMT expression/*INSR* deletion with doxycycline, and throughout to the endpoint.

Fasting blood glucose levels of *MTB:MIC INSR* mice on HFD increased relative to their HFD counterparts, without reaching statistical significance (**Figure 5C**). In this mouse model, exposure to HFD did not lead to increased tumorigenicity, judged by the number and weight of mammary tumors, and lung metastases (**Figures 5D-F**). Nevertheless, under conditions of caloric excess caused by HFD, deletion of one or both copies of *INSR* resulted in reduction of tumour burden in *MTB:MIC INSR* mice by all three criteria, comparable to that seen in the same mice on a normal diet.

INSR-deficient tumors maintain PI3K/Akt and Ras/Erk signaling pathway activity

To gain better insight on how INSR signaling regulates mammary tumourigenesis *in vivo*, immunoblotting of tumor lysates and immunohistochemistry of tumor tissue sections collected at endpoint were performed in both models (**Figure 6**; **Supplementary Figures 4** and **5**). Immunoblotting for signaling pathway activity in tumour lysates failed to yield consistent output (**Supplementary Figure 5A**), thought to

be affected by the presence of stromal and other non-tumour tissue content in tumour isolates.

To quantitatively assess the collected tumour tissue biology, immunohistochemically stained sections of endpoint tumours were digitized (**Supplementary Figures 4A-C**) and analyzed by semi-automated digital image analysis using QuPath bioimage analysis software[36]. Briefly, QuPath was used to identify nuclear and membranous boundaries, detect DAB staining intensity, and perform tissue/tumour classification of individual cells within digital images of stained sections. Following QuPath-assisted exclusion of non-tumour tissues, intensity of each stain for tissues classified as tumour was expressed as H-scores and % Positivity (**Figures 6A-E**; **Supplementary Figures 5B-F**). In agreement with their genotype, QuPath analysis revealed that tumour-specific cells of *MTB:MIC INSR* (F/F) and *NIC INSR* (F/F) mice had greatly diminished INSR staining relative to their *INSR* (+/+) counterparts, with the tumour cells of mice heterozygous for *INSR* loss (F/+) exhibiting intermediary but non-statistically significant reduction (**Figure 6A**; **Supplementary Figure 5B**). Consistent with no impact on tumour progression, Ki67 staining, a marker of active proliferation in tumour cells remained comparable at endpoint across *INSR* genotypes of both models (**Figure 6E**; **Supplementary Figure 5F**). This was paralleled by analogous lack of significant change in levels of phosphorylated AKT (**Figure 6C**; **Supplementary Figure 5D**) and phosphorylated ERK (**Figure 6D**; **Supplementary Figure 5E**). Potential compensatory changes in insulin-like growth factor 1 receptor (IGF1R, an INSR sister receptor capable of transmitting insulin signals) levels in response to genetic *INSR* disruption were also tested by IHC to reveal no difference

between genotypes (**Figure 6B**; **Supplementary Figure 5B**). Of note, *NIC INSR* (F/+) tumours displayed statistically significant reduction of both IGF1R and p-AKT, an observation of likely limited biological significance, as it was not accompanied by decreased proliferative signal, nor did it track with further reduction in INSR levels in *NIC INSR* (F/F) tumours. Judging by immunohistochemistry for the pan-immune marker CD45, there was no difference between *INSR* genotypes in the general immune infiltrates in *MTB:MIC* tumours collected at 10 weeks post-doxycycline induction (**Figure 6F**).

Discussion

Human epidemiological and observational studies have defined a strong correlation between excess body weight and incidence and burden of many cancers, including BC. Obesity is a key driver in cardiovascular, musculoskeletal and kidney diseases, as well as a causal factor in the development of T2D[37]. The rapidly rising global prevalence of obesity makes it one of the greatest threats to human health in the 21st century. There are a number of systemic and molecular mechanisms implicated in mediating the harmful effects of obesity on human health, including the development of cancers[38]. Coupled with broad expression of INSR in human cancers (**Figure 1**), hyperinsulinemia, which correlates with worse BC outcomes[7,39,40], is one of the strongest obesity corollaries thought to contribute to cancer burden (reviewed in [41]).

Using two well-defined genetically engineered mouse models of BC driven by the PyMT and Her2 oncogenes, respectively, we directly probed the importance of the INSR to the development of mammary tumours by its coordinate genetic deletion in

tumour tissue. Transcriptional profiling classifies PyMT mammary tumors with the human BC luminal B subtype[42], whereas mammary tumours in the Her2 transgene model recapitulate many of the features of Her2-positive human BCs[43]. Control tumours from both models express INSR (**Figures 2F-G**), a feature found in >80% of human BC[17,18].

In both models, deletion of a single or both INSR copies dramatically attenuated tumor onset, leading to reduced tumor burden at endpoint (**Figure 3**). Comparable outcome was also reached in the PyMT model under conditions mimicking human obesity leading to hyperglycemia and hyperinsulinemia (**Figure 5D-F**). Longitudinal monitoring of individual tumours in the Her2 model revealed that once tumours appeared, INSR deficiency had no impact on progression or metastasis, indicating that INSR likely participates in the tumour initiation phases.

Mechanistically, mammary tumours driven by PyMT result from association-dependent activation of RTK-proximal effectors of mitogenic PI3K/Akt and Erk signaling pathways[44,45]. The same pathways are also activated by superphysiological transgenesis of Her2[43]. From the tumour analysis at endpoint, INSR loss did not affect proliferation, nor the Akt and Erk signaling throughput, highly representative of a tumour's stage of progression rather than INSR deficiency (**Figures 4** and **6**; **Supplementary Figures 4** and **5**). Complementary studies explored the effects of hyperinsulinemia without obesity on PyMT-driven mouse xenograft growth and found increased insulin-dependent acceleration of the development and progression of tumours[14], whereas the same conditions augmented tumor development and metastasis of Her2-driven xenografts[46], accompanied by hyperactivation of Akt signaling in both

models. Moreover, shRNA-mediated interference with INSR in BC cells in culture led to reduced proliferation and Akt signaling[47,48]. Thus, while hyperinsulinemia can accelerate mammary tumour progression and metastasis in the context of PyMT and Her2 transgenesis in xenografts and INSR deletion can reduce *in vitro* BC cell line growth, presumed diminution of insulin signaling via reduction of INSR levels in mouse mammary gland tumours does not translate to effects on proliferation and Erk/Akt control at later stages of tumorigenesis. The differences between models might be a reflection of a developed insulin/INSR dependence of cultured and xenografted cells while grown *in vitro* and subcutaneously, or distinct tumor heterogeneity in the absence or reduced INSR since inception in the mouse genetically engineered models.

There is evidence that IGF1R and INSR can compensate for each other under conditions of pharmacological intervention or deficiency[47,49], as well as during mouse embryonic development[50]. In our models, levels of IGF1R remained unchanged following INSR loss (**Figure 6C; Supplementary Figure 4E**), suggesting lack of possible compensatory function of IGF1R in maintaining tumour proliferation and Erk/Akt signaling when INSR is reduced/deleted. High proliferation rates and Erk/Akt activity-associated phosphorylation upon INSR loss were paralleled by the unchanged progression indicators in INSR-deficient tumours, with both likely originating from the PyMT and Her2 transgenes. Thus, INSR deletion impacts the early PyMT- and Her2-driven steps towards mammary epithelial transformation and initiation of primary tumours, but not the later phases of progression and metastasis. Carefully designed work aimed towards understanding the earliest steps of mammary transformation, as

well as possible (inter)dependence of INSR expression and activity and that of oncogenic drivers is needed to further define their relationship.

Several lines of evidence suggest that insulin/INSR contribution to tumorigenesis might be particularly prominent in cells/tissues sensitized to insulin action by acquisition of mutations impacting the PI3K/Akt and Ras/Erk signaling pathways (reviewed in[21]). In our model systems, interference with the INSR axis did little to progression or metastasis of tumours caused by major drivers of these pathways, PyMT and Her2, yet had a profound impact on the initiation of tumors and their burden. Projected to management of BC risk in humans, our data highlight the importance of maintaining normal systemic insulin levels, and avoidance of insulin peaks and undiagnosed hyperinsulinemia, as these conditions are likely to favor tumour initiation steps in sensitized cells, where insulin/INSR signaling appears to have a determinant effect. Such view is further supported by the almost identical reduction in tumour burden by deletion of a single copy of INSR in our models, indicative of an insulin dosage threshold for contributions to tumours. While our data indicate that insulin/INSR level pharmacological interference against already developed tumours might be futile, insulin-controlling lifestyle interventions, such as maintenance of lean body weight and physical activity, routine yearly monitoring of fasting insulin levels, and possibly pharmacological reduction of insulin levels in non-diabetics might be beneficial in prevention of cancers of the breast and other organs.

Acknowledgements

We would like to thank the staff in the Animal Research Center at the University Health Network (UHN) for help with animal husbandry and UHN's Applied Molecular Profiling Laboratory for assistance with immunohistochemistry. This work was supported by the Canadian Institutes of Health Research Project Grant (162296) and the Canadian Cancer Society Grant (i2I16-2 grant #704786) to V.S. L.P. is a recipient of The Princess Margaret Hospital Foundation Graduate Fellowships in Cancer Research. Y. P was a recipient of the Canadian BC Foundation postdoctoral fellowship and R. D. of the Banting Postdoctoral Fellowship from the Government of Canada.

Declaration of Interests

The authors have no conflicts of interests to declare.

Author Contributions

Experiments were designed by Y.P., L.P. and V.S. and performed by Y.P., L.P. and S.M. Data, gene expression and statistical analyses was performed by L.P, M.E. and P.S. R.D provided conceptual and technical input. L.P., Y.P. and V.S. wrote the manuscript. All authors discussed the results and commented on the manuscript.

References:

1. World Health Organization. Obesity and Overweight. https://www.who.int/news-room/fact-sheets/detail/obesity-and-overweight (2021).
2. Islami, F., Goding Sauer, A., Gapstur, S. M. & Jemal, A. Proportion of Cancer Cases Attributable to Excess Body Weight by US State, 2011-2015. *JAMA Oncol.* **5**, 384–392 (2019).
3. Calle, E. E., Rodriguez, C., Walker-Thurmond, K. & Thun, M. J. Overweight, Obesity, and Mortality from Cancer in a Prospectively Studied Cohort of U.S. Adults. *N. Engl. J. Med.* **348**, 1625–1638 (2003).
4. Chan, D. S. M. *et al.* Body mass index and survival in women with breast cancer—systematic literature review and meta-analysis of 82 follow-up studies. *Annals of Oncology* vol. 25 1901–1914 (2014).
5. Teras, L. R. *et al.* Sustained Weight Loss and Risk of Breast Cancer in Women 50 Years and Older: A Pooled Analysis of Prospective Data. *J. Natl. Cancer Inst.* **112**, 929–937 (2020).
6. Lazarus, R., Sparrow, D. & Weiss, S. Temporal relations between obesity and insulin: Longitudinal data from the normative aging study. *Am. J. Epidemiol.* **147**, 173–179 (1998).
7. Goodwin, P. J. *et al.* Fasting insulin and outcome in early-stage breast cancer: results of a prospective cohort study. *J Clin Oncol* **20**, 42–51 (2002).
8. Dankner, R., Shanik, M. H., Keinan-Boker, L., Cohen, C. & Chetrit, A. Effect of elevated basal insulin on cancer incidence and mortality in cancer incident patients: The Israel GOH 29-year follow-up study. *Diabetes Care* **35**, 1538–1543

(2012).

9. Kabat, G. C. *et al.* Repeated measures of serum glucose and insulin in relation to postmenopausal breast cancer. *Int. J. Cancer* **125**, 2704–2710 (2009).

10. Gunter, M. J. *et al.* Insulin, insulin-like growth factor-I, and risk of breast cancer in postmenopausal women. *J. Natl. Cancer Inst.* **101**, 48–60 (2009).

11. Hemkens, L. G. *et al.* Risk of malignancies in patients with diabetes treated with human insulin or insulin analogues: A cohort study. *Diabetologia* **52**, 1732–1744 (2009).

12. Heuson, J. C., Legros, N. & Heimann, R. Influence of insulin administration on growth of the 7,12-dimethylbenz(a)anthracene-induced mammary carcinoma in intact, oophorectomized, and hypophysectomized rats. *Cancer Res.* **32**, 233–238 (1972).

13. Heuson, J. C. & Legros, N. Influence of Insulin Deprivation on Growth of the 7,12-Dimethylbenz(a)anthracene-induced Mammary Carcinoma in Rats Subjected to Alloxan Diabetes and Food Restriction. *Cancer Res.* **32**, 226–232 (1972).

14. Novosyadlyy, R. *et al.* Insulin-mediated acceleration of breast cancer development and progression in a nonobese model of type 2 diabetes. *Cancer Res.* **70**, 741–751 (2010).

15. Fierz, Y., Novosyadlyy, R., Vijayakumar, A., Yakar, S. & LeRoith, D. Insulin-sensitizing therapy attenuates type 2 diabetes-mediated mammary tumor progression. *Diabetes* **59**, 686–693 (2010).

16. Zhang, A. M. Y. *et al.* Endogenous Hyperinsulinemia Contributes to Pancreatic Cancer Development. *Cell Metabolism* vol. 30 403–404 (2019).

17. Law, J. H. *et al.* Phosphorylated insulin-like growth factor-i/insulin receptor is present in all breast cancer subtypes and is related to poor survival. *Cancer Res* **68**, 10238–10246 (2008).

18. Mulligan, A. M., O'Malley, F. P., Ennis, M., Fantus, I. G. & Goodwin, P. J. Insulin receptor is an independent predictor of a favorable outcome in early stage breast cancer. *Breast Cancer Res Treat* **106**, 39–47 (2007).

19. White, M. F. & Kahn, C. R. Insulin action at a molecular level – 100 years of progress. *Molecular Metabolism* vol. 52 (2021).

20. Vella, V., Milluzzo, A., Scalisi, N. M., Vigneri, P. & Sciacca, L. Insulin receptor isoforms in cancer. *International Journal of Molecular Sciences* vol. 19 (2018).

21. Hopkins, B. D., Goncalves, M. D. & Cantley, L. C. Insulin–PI3K signalling: an evolutionarily insulated metabolic driver of cancer. *Nature Reviews Endocrinology* vol. 16 276–283 (2020).

22. Yuan, T. L. & Cantley, L. C. PI3K pathway alterations in cancer: variations on a theme. *Oncogene* **27**, 5497–5510 (2008).

23. Saltiel, A. R. Insulin signaling in health and disease. *Journal of Clinical Investigation* vol. 131 (2021).

24. Koboldt, D. C. *et al.* Comprehensive molecular portraits of human breast tumours. *Nature* **490**, 61–70 (2012).

25. Weinstein, J. N. *et al.* The cancer genome atlas pan-cancer analysis project. *Nat. Genet.* **45**, 1113–1120 (2013).

26. Barretina, J. *et al.* The Cancer Cell Line Encyclopedia enables predictive modelling of anticancer drug sensitivity. *Nature* **483**, 603–607 (2012).

27. Goldman, M. J. *et al.* Visualizing and interpreting cancer genomics data via the Xena platform. *Nature Biotechnology* vol. 38 675–678 (2020).

28. Soule, H. D. *et al.* Isolation and Characterization of a Spontaneously Immortalized Human Breast Epithelial Cell Line, MCF-10. *Cancer Res.* **50**, 6075–6086 (1990).

29. Belfiore, A., Frasca, F., Pandini, G., Sciacca, L. & Vigneri, R. Insulin receptor isoforms and insulin receptor/insulin-like growth factor receptor hybrids in physiology and disease. *Endocr Rev* **30**, 586–623 (2009).

30. Gunther, E. J. *et al.* A novel doxycycline-inducible system for the transgenic analysis of mammary gland biology. *FASEB J.* **16**, 283–292 (2002).

31. Rao, T. *et al.* Inducible and coupled expression of the polyomavirus middle T antigen and Cre recombinase in transgenic mice: An in vivo model for synthetic viability in mammary tumour progression. *Breast Cancer Res.* **16**, (2014).

32. Ursini-Siegel, J. *et al.* ShcA signalling is essential for tumour progression in mouse models of human breast cancer. *EMBO J.* **27**, 910–920 (2008).

33. Bates, D., Mächler, M., Bolker, B. M. & Walker, S. C. Fitting linear mixed-effects models using lme4. *J. Stat. Softw.* **67**, 1–48 (2015).

34. Dowling, R. J. O. *et al.* Metformin Pharmacokinetics in Mouse Tumors: Implications for Human Therapy. *Cell Metab.* **23**, 567–568 (2016).

35. Hu, S. *et al.* Dietary Fat, but Not Protein or Carbohydrate, Regulates Energy Intake and Causes Adiposity in Mice. *Cell Metab.* **28**, 415-431.e4 (2018).

36. Bankhead, P. *et al.* QuPath: Open source software for digital pathology image analysis. *Sci. Rep.* **7**, (2017).

37. Blüher, M. Obesity: global epidemiology and pathogenesis. *Nature Reviews*

Endocrinology vol. 15 288–298 (2019).

38. Heymsfield, S. B. & Wadden, T. A. Mechanisms, Pathophysiology, and Management of Obesity. *N. Engl. J. Med.* **376**, 254–266 (2017).

39. Bruning', P. F. ~ *et al. INSULIN RESISTANCE AND BREAST-CANCER RISK*. *Int. J. Cancer* vol. 52 (1992).

40. Cowey, S. & Hardy, R. W. The metabolic syndrome: A high-risk state for cancer? *American Journal of Pathology* vol. 169 1505–1522 (2006).

41. Poloz, Y. & Stambolic, V. Obesity and cancer, a case for insulin signaling. *Cell Death Dis.* **6**, e2037 (2015).

42. Pfefferle, A. D. *et al.* Transcriptomic classification of genetically engineered mouse models of breast cancer identifies human subtype counterparts. *Genome Biol.* **14**, (2013).

43. Simond, A. M. & Muller, W. J. In vivo modeling of the EGFR family in breast cancer progression and therapeutic approaches. in *Advances in Cancer Research* vol. 147 189–228 (Academic Press, 2020).

44. Schaffhausen, B. S. & Roberts, T. M. Lessons from polyoma middle T antigen on signaling and transformation: A DNA tumor virus contribution to the war on cancer. *Virology* vol. 384 304–316 (2009).

45. Attalla, S., Taifour, T., Bui, T. & Muller, W. Insights from transgenic mouse models of PyMT-induced breast cancer: recapitulating human breast cancer progression in vivo. *Oncogene* **40**, 475–491 (2021).

46. Ferguson, R. D. *et al.* Hyperinsulinemia promotes metastasis to the lung in a mouse model of Her2-mediated breast cancer. *Endocr. Relat. Cancer* **20**, 391–

401 (2013).

47. Zhang, H. *et al.* Inhibition of cancer cell proliferation and metastasis by insulin receptor downregulation. *Oncogene* **29**, 2517–2527 (2010).

48. Chan, J. Y., Lapara, K. & Yee, D. Disruption of insulin receptor function inhibits proliferation in endocrine-resistant breast cancer cells. *Oncogene* **35**, 4235–4243 (2016).

49. Buck, E. *et al.* Compensatory Insulin Receptor (IR) Activation on Inhibition of Insulin-Like Growth Factor-1 Receptor (IGF-1R): Rationale for Cotargeting IGF-1R and IR in Cancer. (2010) doi:10.1158/1535-7163.MCT-10-0318.

50. Louvi, A., Accili, D. & Efstratiadis, A. Growth-promoting interaction of IGF-II with the insulin receptor during mouse embryonic development. *Dev. Biol.* **189**, 33–48 (1997).

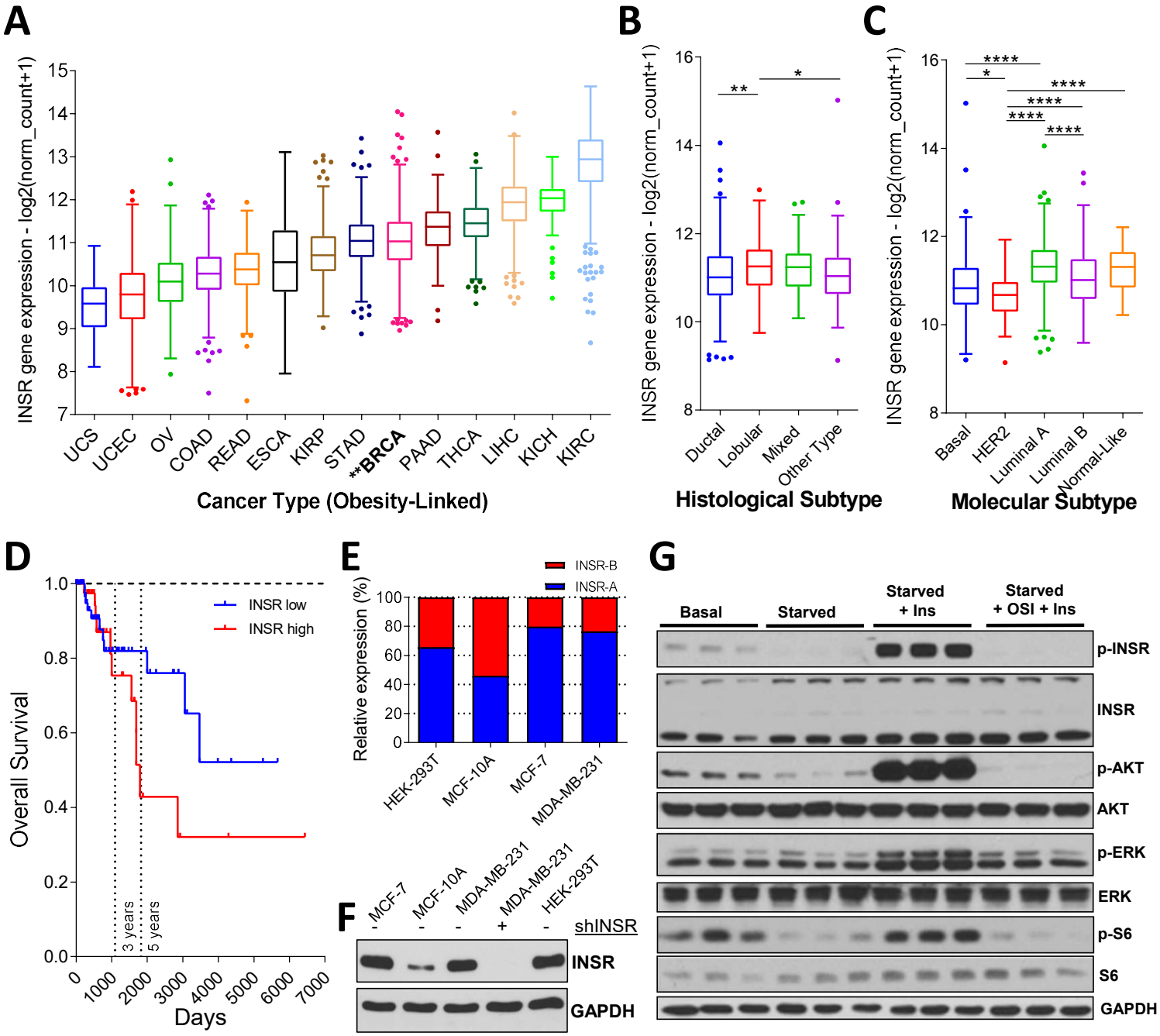

Figure 1: ***INSR expression in breast cancer***. (**A**) RNASeq expression analysis of INSR in obesity-linked cancer types from the TCGA PANCAN dataset[25] in UCSC Xena Functional Genomics Explorer[27]. Breast cancer (BRCA) is highlighted; see Supplementary Table 1 for other cancer type abbreviations. (**B**) RNASeq expression analysis of INSR by histological subtype from TCGA Breast dataset[24] in UCSC Xena Functional Genomics Explorer. Ductal = invasive ductal carcinoma (IDC); Lobular = invasive lobular carcinoma (ILC); Mixed = mixed IDC and ILC. (**C**) RNASeq expression analysis of INSR by molecular subtype from TCGA Breast dataset in UCSC Xena Functional Genomics Explorer. (**D**) Kaplan-Meier analysis of overall survival of patients with basal breast tumours, stratified by INSR expression (INSR high = above median, INSR low = below median; median 11.04) in primary breast tumours, as measured by RNASeq from the TCGA Breast dataset in UCSC Xena Functional Genomics Explorer. (**E**) qRT-PCR analysis showing relative expression of INSR-A and INSR-B isoforms in HEK-293T, MCF-10A, MCF-7 and MDA-MB-231 cell lines. (**F**) Western blot analysis of INSR expression in HEK-293T, MCF-7 and MDA-MB-231 and MCF-10A cell lines. MDA-MB-231 cells were transduced with an shRNA targeting INSR to demonstrate specificity. Blots were probed with antibodies against INSR and GAPDH. (**G**) Western blot analysis of MCF-10A cells grown in supplemented DMEM/HAM (Basal) or starved overnight in the absence of insulin and FBS (Starved), and then either stimulated with 100 nM insulin for 5 minutes (Starved+Ins) or pre-treated with 1 μM OSI-906 for 2 hours before stimulation with 100 nM insulin for 5 minutes (Starved+OSI+Ins). Blots were probed with antibodies to determine both total and phosphorylated levels of INSR, AKT, ERK and S6. GAPDH was used as a loading control. * $p \leq 0.05$, ** $p \leq 0.01$, **** $p \leq 0.0001$; Student's t-test.

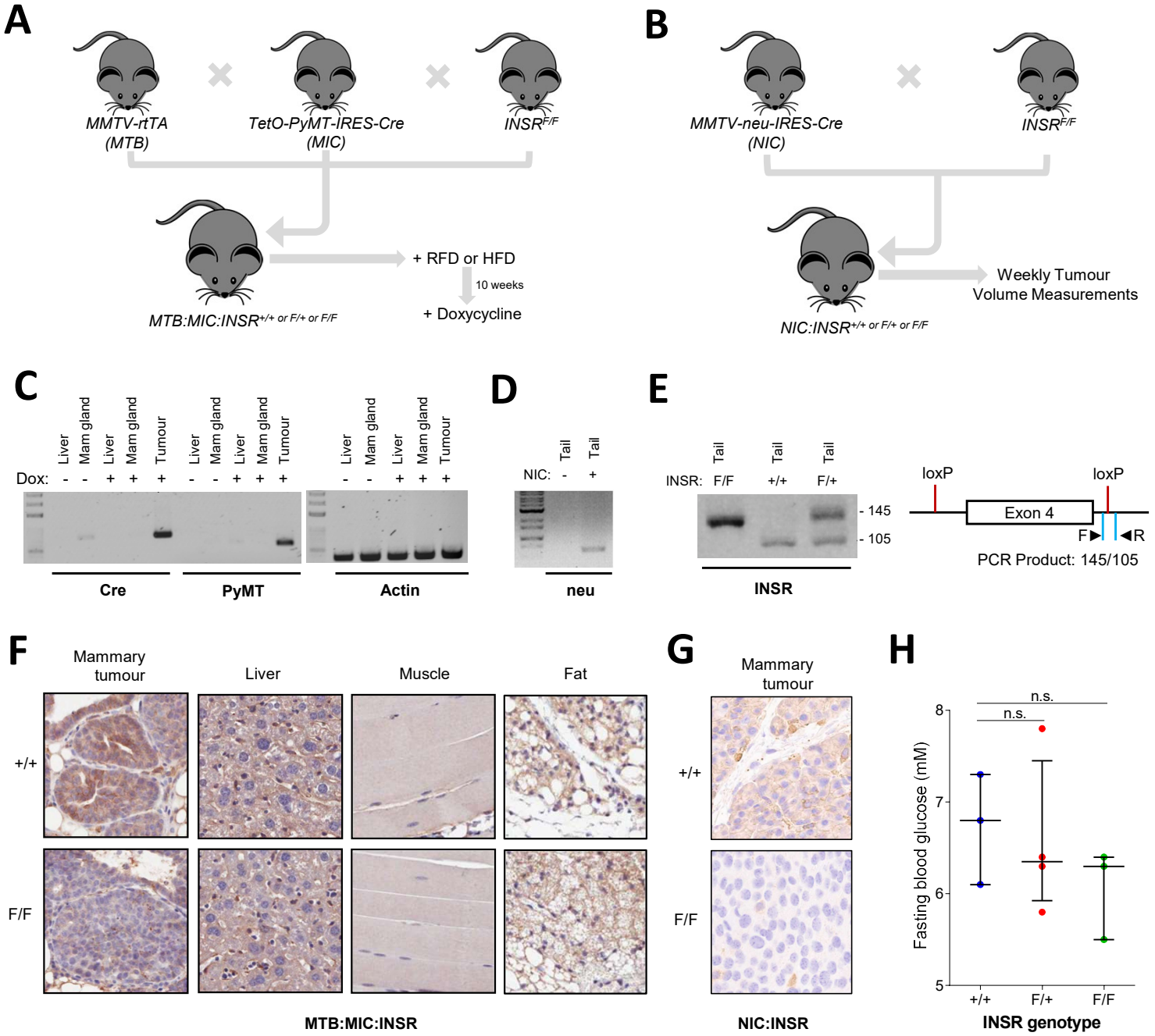

Figure 2: ***Generation of genetic mouse models of breast cancer with conditional deletion of INSR.*** (**A**) Breeding schematic for *MTB:MIC* mice that are either wild-type (+/+), heterozygous (F/+) or homozygous (F/F) for the conditional *INSR* allele. 10 week old mice were fed either regular fat (RFD) or high fat (HFD) diets for an additional 10 weeks, followed by treatment with 2 mg/ml doxycycline to induce mammary tissue-specific expression of the PyMT oncogene with coordinate deletion of *INSR*. (**B**) Breeding schematic for *NIC* mice that are either wild-type (+/+), heterozygous (F/+) or homozygous (F/F) for the conditional *INSR* allele. Tumour measurements were performed weekly and mice were sacrificed at humane endpoint. (**C**) Agarose gel image of RT-PCR showing tissue-specific Cre and PyMT expression upon doxycycline administration in the mammary tumours of *MTB:MIC* mice. (**D**) Agarose gel image of RT-PCR showing the genotyping of *NIC* positive (+) and negative (-) mice. (**E**) Agarose gel showing INSR exon 4 excision in $INSR^{F/+}$ (F/+) and $INSR^{F/F}$ (F/F) mice, followed by the schematic of the PCR strategy. Mice that are wild-type for *INSR* (+/+) are included as a control. (**F**) Immunohistochemical analysis of INSR expression in mammary gland, liver, muscle and fat tissues of *MTB:MIC* mice that are either wild-type (+/+) or homozygous (F/F) for the conditional *INSR* allele. (**G**) Immunohistochemical analysis of INSR expression in the mammary gland of *NIC* mice that are either wild-type (+/+) or homozygous (F/F) for the conditional *INSR* allele. (**H**) Scatterplot of fasting blood glucose levels in *FVB* (+/+, n = 3), *MTB:MIC INSR* (F/+) (n = 4) and *MTB:MIC INSR* (F/F) (n = 3) model mice. Scatterplots show the median and interquartile range. n.s = non-significant; Student's t-test.

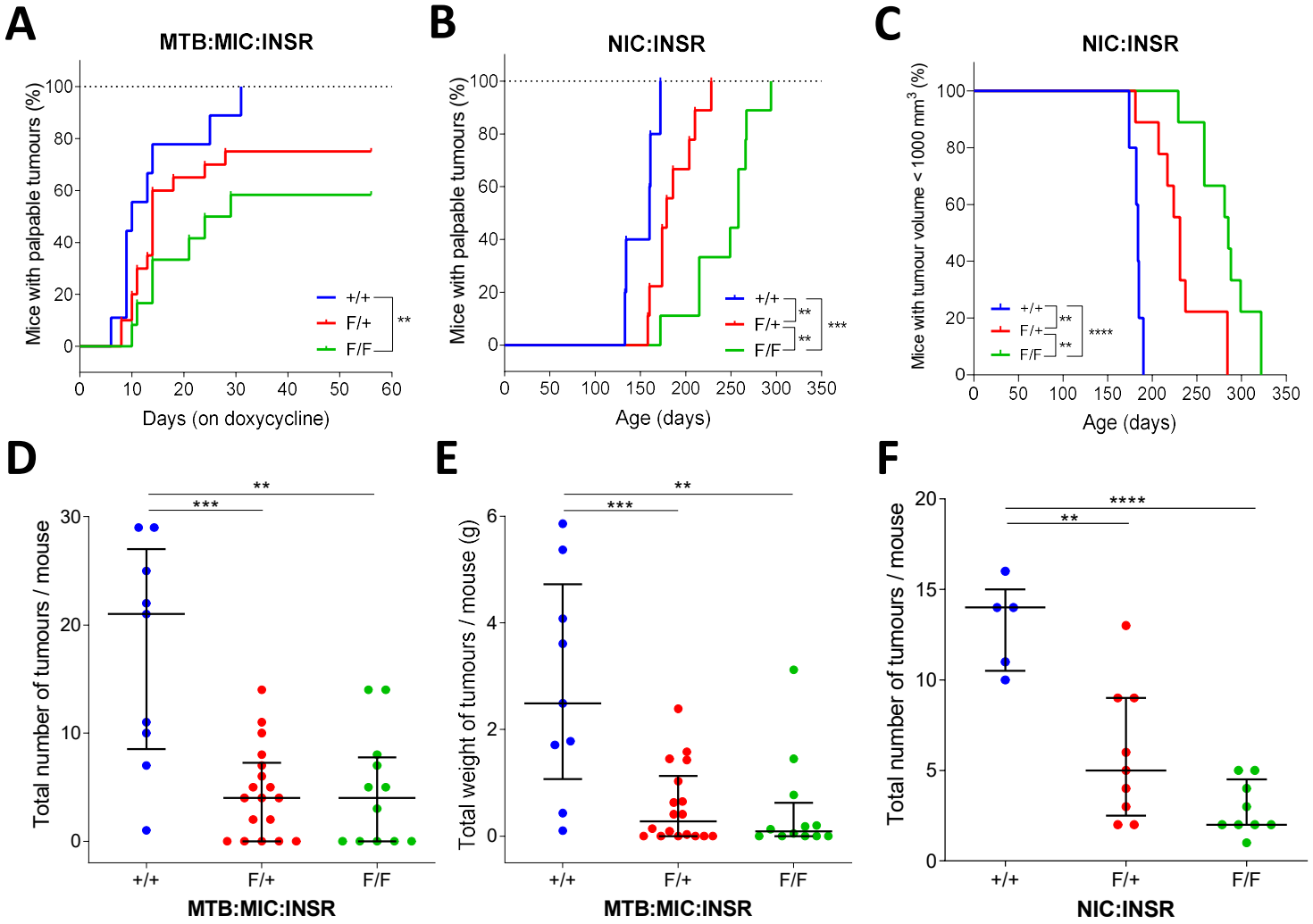

Figure 3*: Loss of INSR delays mammary tumour onset, prolongs survival and reduces tumour burden in vivo.* (**A**) Reverse Kaplan-Meier analysis of mammary tumour onset (post-doxycycline regimen initiation) in *MTB:MIC* mice with wild-type *INSR* alleles (+/+, n = 9) and mice heterozygous (F/+, n = 20) and homozygous (F/F, n = 12) for the conditional *INSR* allele. (**B**) Reverse Kaplan-Meier analysis of mammary tumour onset in *NIC* mice with wild-type *INSR* alleles (+/+, n = 5) and mice heterozygous (F/+, n = 9) and homozygous (F/F, n = 9) for the conditional *INSR* allele. (**C**) Kaplan-Meier analysis of overall survival (i.e. total tumour volume less than 1000 mm^3) in *NIC* mice with wild-type *INSR* alleles (+/+, n = 5) and mice heterozygous (F/+, n = 9) and homozygous (F/F, n = 9) for the conditional *INSR* allele. (**D-E**) Scatterplots of endpoint tumour burden in *MTB:MIC INSR* mice (+/+, n = 9; F/+, n = 18; F/F, n =12) Mice were sacrificed at 8 weeks post-doxycycline treatment regimen initiation, followed by quantification of (**D**) total tumour number and (**E**) total tumour weight. (**F**) Scatterplot of endpoint tumour burden in *NIC INSR* mice (+/+, n = 5; F/+, n = 9; F/F, n = 9). Mice were sacrificed at humane endpoint (tumour volume exceeding 1000 mm^3), followed by quantification of total tumour number. Scatterplots show the median and interquartile range. * $p \leq 0.05$, ** $p \leq 0.01$, *** $p \leq 0.001$, **** $p \leq 0.0001$; log-rank test (**A-C**), Student's t-test (**D-F**).

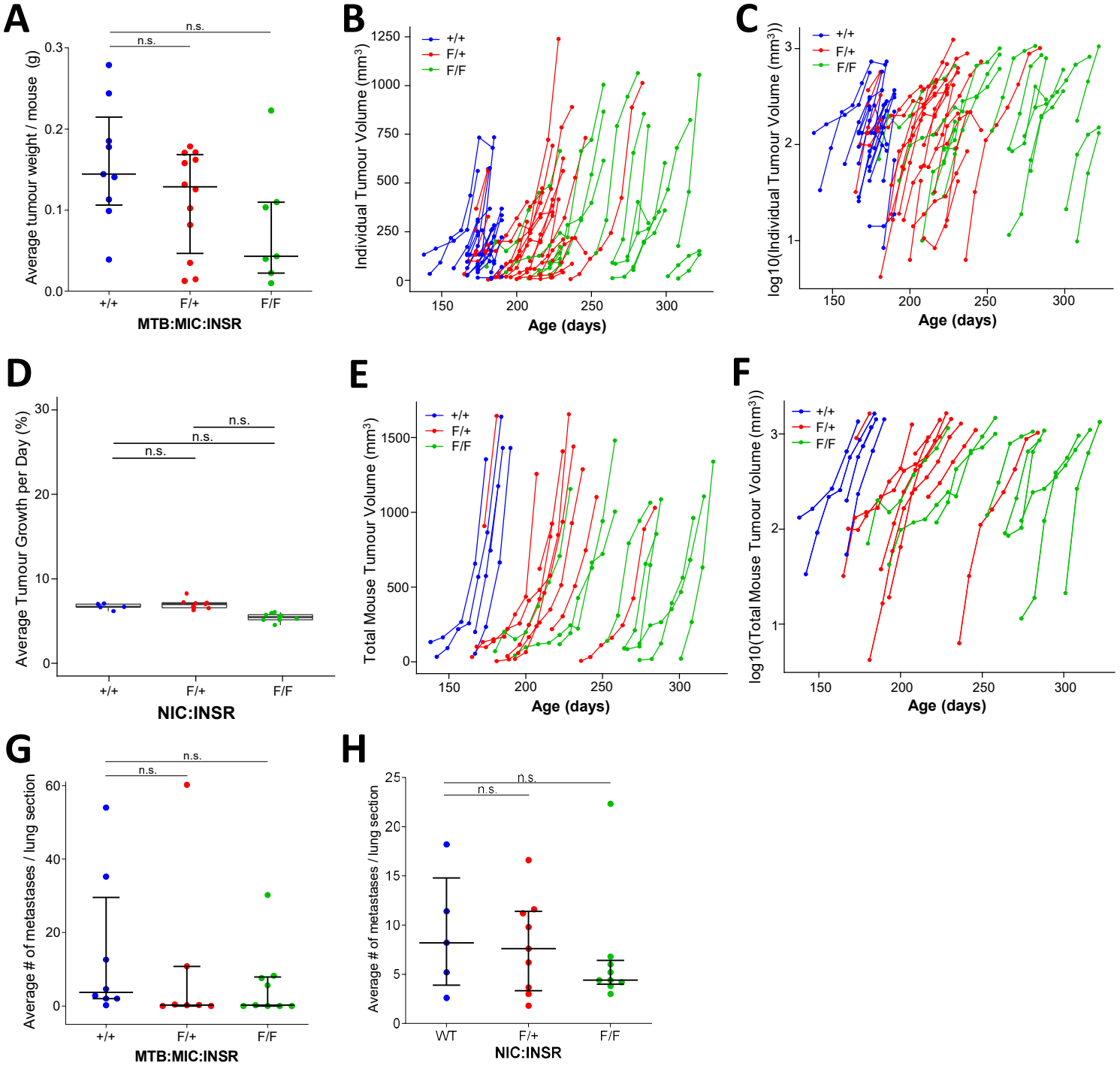

Figure 4: ***Loss of INSR does not affect tumour progression or metastases in vivo.*** (**A**) Scatterplot of average weights of tumours at endpoint in *MTB:MIC INSR* mice which developed tumours by 8 weeks post-doxycycline induction. (**B-C**) Individual tumour growth curves for tumours in *NIC INSR* mice (+/+, n = 21; F/+, n = 24; F/F, n = 18) as a function of the age of the mouse in days, with tumour volume measurements displayed on (**B**) linear and (**C**) logarithmic scale. (**D**) Boxplot of estimated average % tumour growth per day for each *NIC INSR* mouse (+/+, n = 5; F/+, n = 9; F/F, n = 9). Estimates were calculated by adding together average growth rate for each genotype, and any estimated random variation from this average for each mouse. Values for each individual mouse are plotted over the boxplots. (**E-F**) Total tumour burden as measured by summing total volume of each tumour per mouse for *NIC INSR* mice (+/+, n = 5; F/+, n = 9; F/F, n = 9) as a function of the age of the mouse in days, with tumour volume measurements displayed on (**E**) linear and (**F**) logarithmic scale. (**G-H**) Scatterplots of metastatic burden in (**G**)*MTB:MIC INSR* mice (+/+, n = 8; F/+, n = 7; F/F, n = 9) and (**H**) *NIC INSR* mice (+/+, n = 5; F/+, n = 9; F/F, n = 9). Mice were sacrificed at their respective endpoints (see **Figure 3**) and metastatic burden was assessed through quantification of the number of lung metastases as determined by H&E staining of FFPE lung sections, averaged across 5 sections.. Scatterplots show the median and interquartile range. Boxplots show the median and interquartile range, with Tukey style whiskers. n.s = non-significant; Student's t-test (**A, G-H**), ANOVA (**D**).

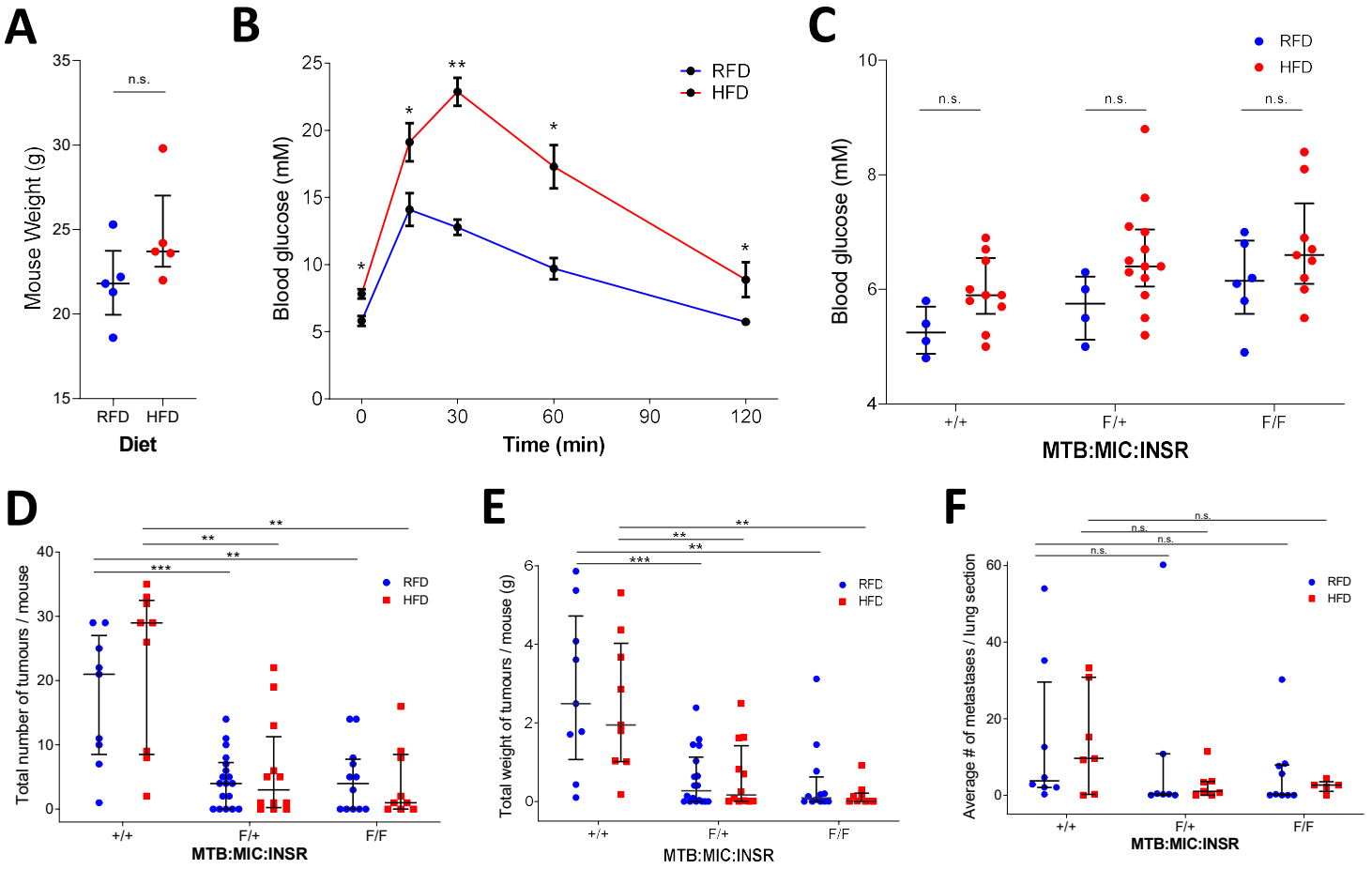

Figure 5: ***Impact of INSR loss persists in conditions which recapitulate obesity and hyperinsulinemia.*** (**A-B**) Scatterplots of (**A**) total body weight measurements and (**B**) time-resolved plot of intraperitoneal glucose tolerance test (2 g/Kg) performed on *FVB* mice fed either RFD (n = 5) or HFD (n = 5), followed by fasting for 6 h. (**C-F**) Scatterplots of blood glucose, endpoint tumour burden and metastatic burden of *MTB:MIC INSR* mice treated with regular fat diet (RFD) or high fat diet (HFD) for 10 weeks prior to 8-week doxycycline regimen initiation followed by sacrifice. Endpoint (**C**) basal blood glucose concentrations (*for RFD*, +/+, n = 4; F/+, n = 4; F/F, n = 6; *for HFD*, +/+, n = 10; F/+, n = 13; F/F, n = 9), (**D**) tumour number (*for RFD*, +/+, n = 9; F/+, n = 18; F/F, n = 12; *for HFD*, +/+, n = 9; F/+, n = 12; F/F, n = 9), (**E**) tumour weight (*for RFD*, +/+, n = 9; F/+, n = 18; F/F, n = 12; *for HFD*, +/+, n = 9; F/+, n = 12; F/F, n = 9), and (**F**) lung metastases (*for RFD*, +/+, n = 8; F/+, n = 7; F/F, n = 9; *for HFD*, +/+, n = 7; F/+, n = 7; F/F, n = 5) were quantified (see **Figures 3 and 4**). Scatterplots show the median and interquartile range. * $p \leq 0.05$, ** $p \leq 0.01$, *** $p \leq 0.001$, n.s. = not significant; Student's t-test.

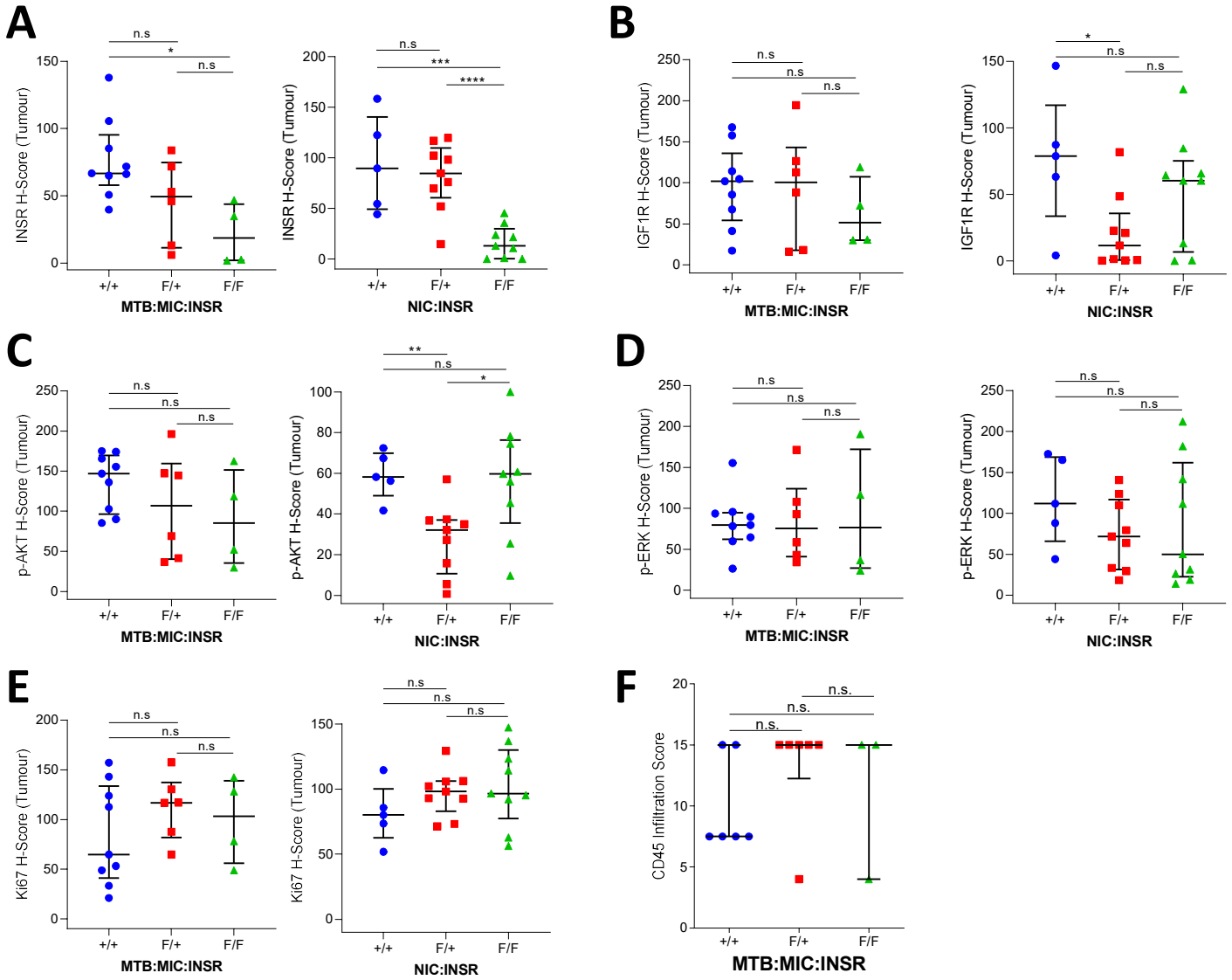

Figure 6: ***Tumours that arise in animals with INSR deficiency display no difference in downstream INSR signaling.*** (**A-E**) Scatterplots of digital pathological analysis by QuPath software of immunohistochemically stained sections of paraffin embedded tumours collected at endpoint from *MTB:MIC INSR* (+/+, n = 9; F/+, n = 6; F/F, n = 4) and *NIC INSR* (+/+, n = 5; F/+, n = 9; F/F, n = 9) mice. H-scores for scanned images of stained tumour sections were determined by QuPath using *Simple Tissue Detection* followed by *Positive Cell Detection* and tissue classification, which selectively scored individual tumour cells as positive (1+, 2+ or 3+) or negative for staining of (**A**) INSR, (**B**) IGF1R, (**C**) phospho-AKT, (**D**) phosphor-ERK, and (**E**) Ki67. (**F**) Scatterplot of CD45 infiltration score of tumours collected from *MTB:MIC INSR* mice (+/+, n = 6; F/+, n = 6; F/F, n = 3) following 10-week doxycycline induction. Scatterplots show the median and interquartile range. * $p \leq 0.05$, ** $p \leq 0.01$, *** $p \leq 0.001$, **** $p \leq 0.0001$, n.s. = not significant; Student's t-test.